

SINGLE-PIXEL CAMERA SENSING MATRIX DESIGN FOR HIERARCHICAL COMPRESSED SPECTRAL CLUSTERING

Carlos Hinojosa , Jorge Bacca, Edwin Vargas, Sergio Castillo, and Henry Arguello

Department of Computer Science, Universidad Industrial de Santander
Bucaramanga, 680002, Colombia

ABSTRACT

Compressive spectral imaging (CSI) acquires random projections of a spectral scene. Typically, before applying any post-processing task, e.g. clustering, it is required a computationally expensive reconstruction of the underlying 3D scene. Therefore, several works focus on improving the reconstruction quality by adaptively designing the sensing matrix aiming at better post-processing results. Instead, this paper proposes a hierarchical adaptive approach to design a sensing matrix of the single pixel camera, such that pixel clustering can be performed in the compressed domain. Specifically, in each step of the hierarchical model, a sensing matrix is designed such that clustering features can be extracted directly from the compressed measurements. Finally, the complete segmentation map is obtained with the majority voting method in the partial clustering results at each hierarchy step. In general, an overall accuracy of 78.94%, and 65.35 % was obtained using the “Salinas”, and “Pavia University” spectral image datasets, respectively.

Index Terms— compressive spectral clustering, single pixel camera, hierarchical clustering, matrix design

1. INTRODUCTION

Spectral imaging (SI) acquires two-dimensional spatial information of a scene across a range of spectral wavelengths. Compared to traditional RGB imaging systems, SI provides more information about the pixels in the scene, which allows the identification of several features of the target [1]. Exploiting this fact, SI has emerged as a valuable tool for remote sensing classification where the goal is to assign a group or class to each pixel of the scene [2]. In particular, spectral clustering methods have been successfully employed to spectral image classification when the labeled samples are unavailable or difficult to acquire [2]. On the other hand, the classification task usually improves as the number of spectral bands increases [3]. However, this requires sensing more information, which makes spectral data acquisition and processing a

challenging problem under traditional scanning-based methods.

Recently, compressive spectral imaging (CSI) has emerged as a SI approach that acquires compressed projections of the whole data cube instead of direct measurement of all the voxels. This allows to detect and reduce the dimensionality of the scene in a single step. Consequently, the cost of storing, and processing spectral images using CSI devices is significantly reduced [4, 5]. To recover the spectral image from the compressed measurements, different optimization algorithms that solve the underlying ill-posed problem have been employed. To name a few, the fast iterative shrinkage-thresholding algorithm (FISTA) [6], the gradient projection for sparse representation (GPSR) [7], or the orthogonal matching pursuit (OMP) [8] are state-of-the-art recovery algorithms. Although the optimization algorithms mentioned above provide good performance, they are computationally expensive and presents slow converge, which limits CSI in terms of time [9, 10].

On the other hand, different works have focused on adaptively designing the set of coding patterns for CSI, with the objective of better reconstructions that benefit post-processing results [11]. However, recent works have shown that post-processing tasks such as classification [12], clustering [13], and unmixing [14] can be performed directly on the compressive domain bypassing the signal recovery stage. For instance, [13] shows that it is possible to employ sparse subspace clustering directly from 3D-CASSI[15] measurements acquired with a carefully designed matrix, which preserves the subspace structure.

In this work, we propose a hierarchical approach to design a sensing matrix of the single pixel camera (SPC) [16] such that clustering features are extracted directly from the acquired compressed measurements. Specifically, at each level of the hierarchy, a sensing matrix is designed as the product of a Hadamard matrix and a decimation matrix. This decomposition allows obtaining a set of features directly from the compressed measurements exploiting the properties of the Hadamard matrix.

In the proposed approach, the decimation matrix at a given level is designed to group similar features of the previous level in segments. Therefore, the composite sensing

Corresponding Author Email: carlos.hinojosa@saber.uis.edu.co.

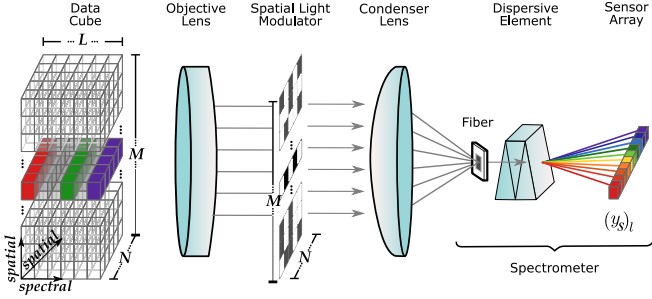


Fig. 1. Sensing process of the single pixel camera (SPC) with a point spectrometer.

matrix has less sampling vectors and it is intended to provide fewer and more compact features than those obtained in the previous level. For this work the decimation matrix is obtained using the k-means algorithm, however, other alternatives can be employed. Finally, a complete segmentation map is obtained by performing majority voting on the partial clustering results obtained using the set of features of each hierarchy level. In general, an overall accuracy of 78.94%, and 65.35 % was obtained using the “Salinas”, and “Pavia University” spectral image datasets, respectively.

2. CSI ACQUISITION SYSTEM

2.1. SPC Sensing Model

The proposed CSI classification approach in this paper is performed on the compressed measurements acquired with the single-pixel camera (SPC), which employs a point spectrometer to obtain the spectral information [16]. Figure 1 depicts the components and sensing process of the adopted SPC architecture. Specifically, the objective lens focuses the input 3D scene \mathcal{F} , with L spectral bands and $M \times N$ spatial pixels, onto the coded aperture $\mathbf{T} \in \mathbb{R}^{M \times N}$, that spatially modulates each spectral pixel. The coded aperture \mathbf{T} can be modeled as a binary pattern, that blocks the light or lets it pass through each pixel. In this work, these binary levels are either 1 and -1 , where the modulation effect caused by the -1 entries can be practically implemented using an all ones coded aperture measurement and subtract it from each captured snapshot [17]. Then, the coded scene passes through the condenser lens, which concentrates the light to a single spatial point, that contains all the encoded data. Finally, a single point Whisk-broom spectrometer is used as a detector to obtain the spectral information. Mathematically, the discrete sensing process can be modeled as

$$y_l = \sum_{m=1}^M \sum_{n=1}^N T_{m,n} \mathcal{F}_{m,n,l}, \quad (1)$$

for $l = 1 \dots L$, where y_l represents the measurement corresponding to the l -th band. Note that one coded aperture mod-

ulates all spectral bands uniformly, hence, for each band, the sensing process can be rewritten in the standard form of linear equations as

$$y_l = \mathbf{h}^T \mathbf{f}_l, \quad (2)$$

where $\mathbf{h} \in \{1, -1\}^{MN}$ is the vectorization of the coded aperture, given by $\mathbf{h} = [T_{1,1}, T_{2,1}, \dots, T_{M,N}]$, and \mathbf{f}_l is the vector form of the l -th spectral band of \mathcal{F} . Furthermore, it is possible to capture several snapshots by employing a different coded aperture pattern each time. Then, the multi-shot scheme for each band is expressed in matrix form as

$$\mathbf{y}_l = \mathbf{H} \mathbf{f}_l, \quad (3)$$

where $\mathbf{H} \in \mathbb{R}^{K \times MN}$, K is the number of shots, each row of $\mathbf{H} = [\mathbf{h}_1^T, \dots, \mathbf{h}_K^T]$ is the vector form of the coded aperture used on that particular shot, and $\mathbf{y}_l = [y_1, \dots, y_K]^T$.

In general, the sensing model for all spectral bands can be stacked in a single vector as $\mathbf{y} = [\mathbf{y}_1^T \dots \mathbf{y}_L^T]^T$, such that the sensing model can be rewritten as

$$\mathbf{y} = (\mathbf{I}_L \otimes \mathbf{H})[\mathbf{f}_1^T, \dots, \mathbf{f}_L^T]^T = \hat{\mathbf{H}} \mathbf{f}, \quad (4)$$

where $\hat{\mathbf{H}} = \mathbf{I}_L \otimes \mathbf{H}$, is a block diagonal matrix, \mathbf{I}_L represents an $L \times L$ identity matrix, and \otimes denotes the Kronecker product. The compression ratio in this model is given by $\gamma = \frac{K}{MN}$, where $\gamma \in [0, 1]$.

2.2. CSI Reconstruction

Typically, the following step after acquiring the SPC measurements is to recover the underlying spectral scene. Given that the amount of acquired measurements KL is far less than the number of 3D data cube entries to be estimated MNL , the reconstruction problem to be solved becomes ill-posed and, therefore it cannot be solved by directly inverting the system in Eq. 4. The theory of compressive sensing provides an alternative solution method to recover the underlying spectral scene \mathcal{F} from the measurement set \mathbf{y} , assuming that $\mathbf{f} \in \mathbb{R}^{MNL}$ has a \hat{S} -sparse representation in a given basis Ψ and there exists high incoherence between the sensing matrix $\hat{\mathbf{H}}$ and the basis Ψ . Therefore, the measurement set \mathbf{y} in Eq. 4 can be expressed as $\mathbf{y} = \hat{\mathbf{H}} \Psi \theta$, where $\mathbf{f} = \Psi \theta$ and θ is a sparse vector with $\hat{S} \ll MNL$ nonzero entries, such that \mathbf{f} can be approximated as a linear combination of only \hat{S} columns of Ψ . Then, the inverse CS problem consists of recovering θ such that the $\ell_2 - \ell_1$ cost function is minimized, i.e., it looks for a sparse approximation of the spectral data cube. Mathematically, the optimization problem can be written as

$$\tilde{\mathbf{f}} = \Psi \left\{ \arg \min_{\theta} \|\hat{\mathbf{H}} \Psi \theta - \mathbf{g}\|_2^2 + \tau \|\theta\|_1 \right\}, \quad (5)$$

where τ is a regularization constant.

2.3. Sensing Matrix Design

In general, the optimization problem described in Eq. 5 is computationally expensive, and its complexity grows in proportion to the data dimensions. Since several applications require fast spectral image reconstructions, recent works have focused on developing fast, although with low precision, recovery methods [17, 18]. In particular, taking into account the structure of Hadamard matrices, the work in [18] proposes to design the sensing matrix for each band \mathbf{H} as

$$\mathbf{H} = \mathbf{W}\Delta, \quad (6)$$

where $\mathbf{W} \in \{-1, 1\}^{K \times K}$ is a Hadamard matrix, and $\Delta \in \mathbb{R}^{K \times MN}$ is a decimation matrix.

Recently, a fast spectral image recovery method was introduced in [17], where authors proposed to design Δ by obtaining superpixels from an RGB image which was acquired as side information. Specifically, the method named *FMR* takes advantages of the fact that the inverse of a Hadamard matrix is its transpose and perform a fast low-resolution reconstruction for each spectral band as

$$\tilde{\mathbf{f}}_l = (1/K)\hat{\Delta}\mathbf{W}^T\mathbf{y}_l = (1/K)\hat{\Delta}\mathbf{W}^T\mathbf{W}\Delta\mathbf{f}_l \approx \mathbf{f}_l. \quad (7)$$

Note that, instead of performing the complete reconstruction, it is possible to directly extract features from the compressed measurements. In particular, features from the l -th band can be obtained as

$$\bar{\mathbf{f}}_l = \mathbf{W}^T\mathbf{g}_l = \Delta\mathbf{f}_l, \quad (8)$$

where $\bar{\mathbf{f}}_l$ contains the average spectral information of pixels grouped in segments given by the structure of the downsampling matrix Δ . It is important to note that, similar as in [17], in the following sections we assume that $K = N_{seg}$.

3. PROPOSED CSI CLUSTERING

Taking into account, the sensing matrix construction approach presented in Eq. 6, it is possible to design the downsampling matrix Δ to efficiently extract clustering features from the compressed measurements. In this section, we present an unsupervised approach to perform both, Δ matrix design and clustering of the spectral image pixels by directly using the compressed measurements. The complete workflow of the proposed approach is depicted in Fig. 2.

3.1. DownSampling Matrix Design

In general, the binary matrix $\Delta \in \mathbb{R}^{N_{seg} \times MN}$ groups the $M \times N$ spectral pixels in N_{seg} segments, such that each component of the vector $\bar{\mathbf{f}}_l = \Delta\mathbf{f}_l$ contains the average spectral information of pixels grouped in one segment. More formally, denote \mathbf{p}^e as the vector of size n_e containing the indices of all pixels belonging to the e -th segment. Then, the nonzero values of the e -th row of Δ , denoted in vector form as $(\delta_e)^T$,

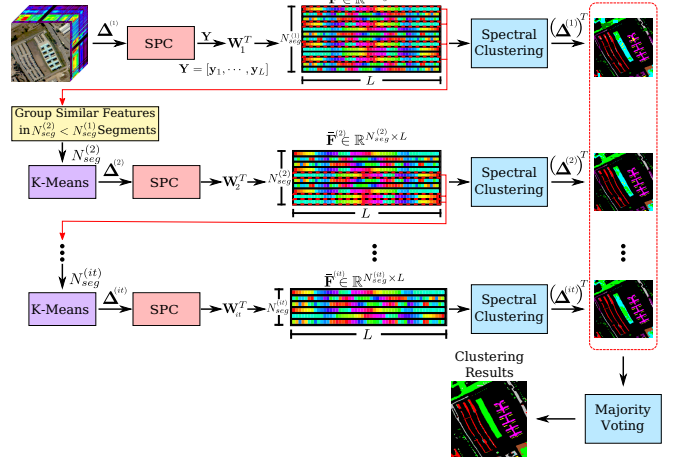


Fig. 2. Workflow of the proposed SPC sensing matrix design and compressed measurements clustering.

Algorithm 1 DownSampling Matrix Design

Input: $N_{seg}, \bar{\mathbf{F}}$
Output: Δ

```

1: procedure DSAMPLING_DESIGN( $\bar{\mathbf{F}}, N_{seg}$ )
2:    $k_{idx} \leftarrow k\text{-means}(\bar{\mathbf{F}}, N_{seg})$   $\triangleright k_{idx}$  contains the segment labels
3:    $\Delta \leftarrow \text{zeros}(N_{seg}, \text{length}(k_{idx}))$ 
4:   for  $e \leftarrow 1$  to  $N_{seg}$  do
5:      $\mathbf{p}^e \leftarrow \text{find}(k_{idx} = e)$ 
6:      $n_e \leftarrow \text{length}(\mathbf{p}^e)$ 
7:     for  $j \leftarrow 1$  to  $n_e$  do
8:        $(\delta_e)_{(\mathbf{p}^e)_j}^T = \frac{1}{n_e}$   $\triangleright$  Update each row of  $\Delta$ 
9:     end for
10:   end for
11:   return  $\Delta$ 
12: end procedure

```

are determined by the entries of \mathbf{p}^e and the value of n_e as follows:

$$(\delta_e)_{(\mathbf{p}^e)_j}^T = \frac{1}{n_e}, \quad \text{for } j = 1, \dots, n_e, \quad (9)$$

where $(\delta_e)_{(\mathbf{p}^e)_j}^T$ denotes the position in δ_e indexed by the j -th entry of the vector \mathbf{p}^e .

The main idea of the proposed design of Δ is to group pixels such that similar spectral information is taken into account. As only the compressed measurements are available, it is proposed to design Δ in an iterative hierarchical fashion such that N_{seg} decreases (more pixels are grouped in one segment) in each iteration and the previous design of Δ is used to redefine the new segments, see Algorithm 1.

In the first iteration, Δ is designed such that all the pixels are grouped in $N_{seg}^{(1)}$ square segments, which are determined without prior information. Once the compressed measurements are acquired, the feature vector $\bar{\mathbf{f}}_l$ is obtained for each spectral band l , hence the feature matrix $\bar{\mathbf{F}}$ is constructed

as

$$\bar{\mathbf{F}} = [\bar{\mathbf{f}}_1, \dots, \bar{\mathbf{f}}_L] \in \mathbb{R}^{N_{seg} \times L}, \quad (10)$$

where the rows contain the average spectral information of each segment. For the next it iterations, N_{seg} is selected as $N_{seg}^{(it)} < N_{seg}^{(it-1)} < \dots < N_{seg}^{(1)}$ and the k -means algorithm is used to find the new segments with inputs $\bar{\mathbf{F}}$ and N_{seg} , as the data matrix and the number of desired clusters, respectively. Then, the \mathbf{p}^e vectors are built for each segment e using the output of k -means, and the new Δ matrix is obtained using the Eq. 9.

3.2. Data Clustering

At each iteration of the main algorithm, the downsampling matrix Δ is constructed and it is used to obtain a partial clustering of the pixels using the Spectral Clustering method. Since, at each iteration, the number of segments N_{seg} is decreased, this approach can be seen as a multiscale clustering of pixels. Furthermore, denoting N_s as the number of scales or levels in the hierarchy, the compression ratio given by using the SPC architecture and the proposed clustering approach can be determined as

$$\tilde{\gamma} = \frac{1}{MN} \sum_{it=1}^{N_s} N_{seg}^{(it)}. \quad (11)$$

In order to perform the data clustering, we construct the similarity graph $\mathbf{G} \in \mathbb{R}^{n \times n}$ using the k -nearest neighbor approach described in [19]. Then, the cluster indices $\bar{\mathbf{C}}$ are obtained by applying the spectral clustering to the similarity graph. Finally, the cluster membership of all the spectral pixels in the full image are obtained by applying the upsampling operator Δ^T onto $\bar{\mathbf{C}}$, see Algorithm 2. Note that both, the similarity graph construction and the spectral clustering computation are performed on the feature matrix $\bar{\mathbf{F}}$. Hence, the proposed approach boosts the computational performance.

Algorithm 2 Data Clustering

Input: $\bar{\mathbf{F}} \in \mathbb{R}^{N_{seg} \times L}$, Δ downsampling matrix, k clusters
Output: Segmentation of the spectral pixels: $\mathbf{F}_1, \dots, \mathbf{F}_k$

```

procedure DATA_CLUSTERING( $\bar{\mathbf{F}}, \Delta, k$ )
2:    $\mathbf{G} \leftarrow \text{Build\_Sim\_Graph}(\bar{\mathbf{F}})$   $\triangleright k$ -nearest neighbor graph
     $\triangleleft \text{Obtain Cluster indices}$ 
4:    $\bar{\mathbf{C}}_{idx} \leftarrow \text{Spectral\_Clustering}(\mathbf{G}, k)$   $\triangleright$  Spectral Clustering [19]
     $\mathbf{C}_{idx} \leftarrow \Delta^T \bar{\mathbf{C}}_{idx}$   $\triangleright$  Upsampling
6: end procedure

```

4. SIMULATIONS AND RESULTS

In this section, the performance of the proposed image classification method is evaluated. In particular, Pavia University and the Salinas Valley data sets were used.

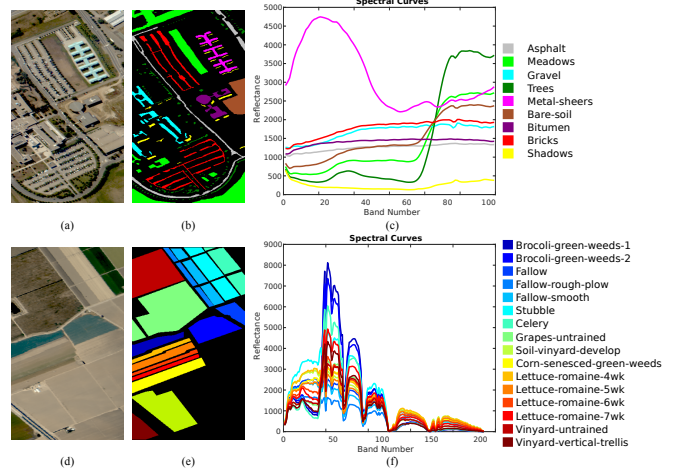


Fig. 3. False-color images (a) and (d), ground truth maps (b) and (e), and land-cover spectral signatures (c) and (f), for Pavia University and Salinas Valley, respectively.

The Pavia University hyperspectral data set was sensed over an urban area in northern Italy, by the Reflective Optics System Imaging Spectrometer (ROSIS-03) airborne sensor. The reference image is a section of 512×192 pixels and 103 spectral bands, with a spatial resolution of 1.3 meters per pixel and a spectral coverage ranging from 0.43 to $0.84 \mu\text{m}$ wavelengths. Pavia University contains nine main land-cover classes: asphalt, meadows, gravel, trees, metal sheets, bare soil, bitumen, bricks, and shadows. Figure 3(a), (b) and (c) shows a false-color version, the ground truth, and the spectral signatures of the dataset, respectively.

The Salinas dataset was collected by the airborne visible/infrared imaging spectrometer (AVIRIS) on Salinas Valley, California, USA. The reference image is also a section of 512×192 pixels and 204 spectral bands in the range of 0.24 to $2.40 \mu\text{m}$. The Salinas ground truth contains 16 land-cover classes: broccoli green weeds 1, broccoli green weeds 2, fallow, fallow rough plow, fallow smooth, stubble, celery, grapes untrained, soil vineyard develop, corn senesced green weeds, lettuce romaine 4 wk, lettuce romaine 5 wk, lettuce romaine 6 wk, lettuce romaine 7 wk, vineyard untrained, and vineyard vertical trellis. The ground truth is shown in Fig. 3 (e), where the spectral signatures of each class are presented in Fig. 3 (f).

The first two experiments were performed to show the sensitivity of the main parameters of the proposed method, i.e., the number of neighbors in the data clustering step and the number of scales or levels in the hierarchy sensing model. In both experiments, the number of segments were fixed as $N_{seg}^{(1)} = 8192$, $N_{seg}^{(2)} = 6144$, $N_{seg}^{(3)} = 4096$, $N_{seg}^{(4)} = 3072$, $N_{seg}^{(5)} = 2048$, and $N_{seg}^{(6)} = 1024$, for $it = 1, \dots, 6$, i.e., the maximum level of hierarchy was 6. In the first experiment, the sensing ratio was fixed to 25%, whose value was obtained

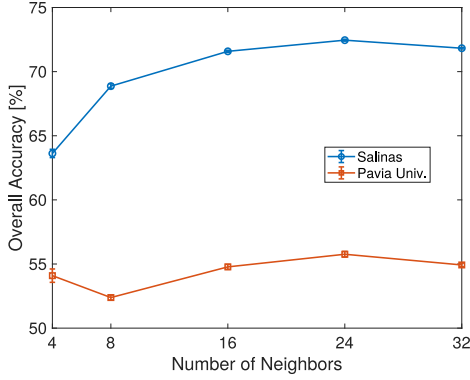


Fig. 4. Overall clustering accuracy as a function of the number of Neighbors in the proposed method

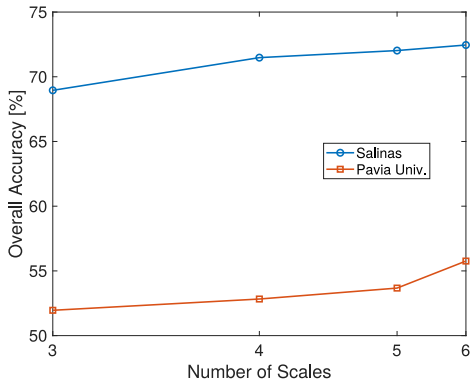


Fig. 5. Overall clustering accuracy as a function of the number of scales in the proposed method

using Eq. 11, and the number of neighbors was varied from 4 to 32. The obtained overall accuracy curve of classification results, along with the mean and variance for each neighbor, is depicted in Fig. 4, where the presented results are the average of 20 trials. It can be observed that the largest variance occurs when using 4 neighbors as well as the best performance is obtained when using 24 neighbors for both datasets. Taking into account the previous results, in the second experiment, the number of neighbors is fixed as 24, and the number of scales was varied from 3 to 6. The obtained results are shown in Fig. 5, where it is observed that as the number of scales increases, the quality of classification improves as expected with the proposed method.

In the last experiment, the results obtained with the proposed method is compared with the approach of using the same hierarchical scheme, but different designs of Δ . The first design, which we refer as “non-designed Δ ”, corresponds to the first level of the proposed hierarchical approach, i.e., Δ is designed such as that all the pixels are grouped in square segments. The second design, which we refer as “FMR+Clustering”, corresponds to the approach described in [17], where Δ is designed using super-pixels obtained from an RGB image which was acquired as side information. Note

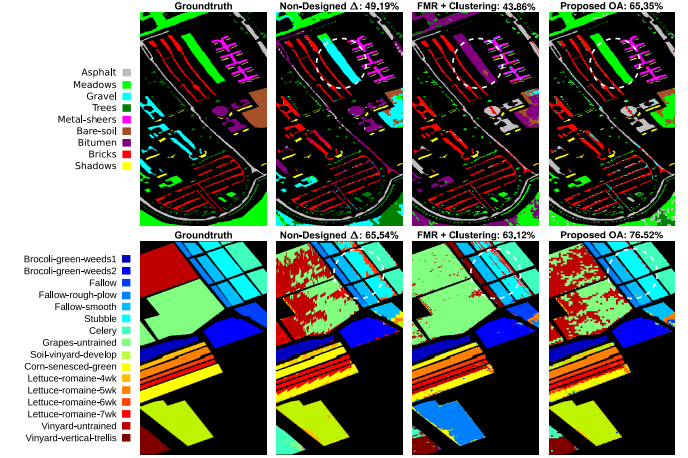


Fig. 6. Visual clustering results on Pavia University (top) and Salinas data sets (bottom). The figure shows the ground truth and the results for the evaluated methods.

that the FMR method requires image reconstruction before performing spectral clustering. Figure 6, and Tables 1 and 2 show the visual and quantitative results obtained with the methods mentioned above. Specifically, tables show the numerical results for each of the land-cover classes (producer’s accuracy), overall accuracy (OA), average accuracy (AA), and Kappa (κ) coefficients [20], where the best value of each row is shown in bold font and the second best is underlined. All the results, except the Kappa coefficients, are given in percentage. As observed, the proposed hierarchical method exhibits the highest increment in classification performance compared to the other approaches. Besides, note that the reconstruction time is avoided.

| Class | Non-Designed Δ | FMR+Clustering | Proposed |
|---------------------------|-----------------------|----------------|--------------|
| Broccoli-green-1 | 98.11 | 98.11 | 98.11 |
| Broccoli-green-2 | <u>98.34</u> | 98.77 | 97.67 |
| Fallow | 7.91 | 74.62 | 8.70 |
| Fallow-rough-plow | 96.48 | 0.00 | 95.91 |
| Fallow-smooth | 92.91 | 96.27 | 93.09 |
| Stubble | <u>90.05</u> | 77.14 | 97.07 |
| Celery | 47.20 | 99.17 | 98.07 |
| Grapes-untrained | <u>78.91</u> | 93.95 | 55.15 |
| Soil-vineyard-develop | 93.42 | 0.48 | 95.74 |
| Corn-senesced-green-weeds | 65.34 | <u>59.43</u> | 50.27 |
| Lettuce-romaine-4wk | <u>19.19</u> | 2.15 | 28.84 |
| Lettuce-romaine-5wk | 0.00 | 100.00 | 99.53 |
| Lettuce-romaine-6wk | 0.00 | 97.71 | 96.51 |
| Lettuce-romaine-7wk | 0.00 | <u>83.27</u> | 89.07 |
| Vineyard-untrained | 0.00 | <u>3.10</u> | 67.94 |
| Vineyard-vertical-trellis | 90.59 | <u>82.79</u> | 77.37 |
| AA | 54.90 | <u>66.68</u> | 78.07 |
| OA | 62.55 | <u>63.12</u> | 76.52 |
| Kappa | 0.58 | <u>0.59</u> | 0.74 |

Table 1. Quantitative Results of different design approaches of Δ for the Salinas Valley Image

| Class | Non-Designed Δ | FMR+Clustering | Proposed |
|--------------|-----------------------|----------------|--------------|
| Asphalt | 61.29 | 91.75 | <u>90.21</u> |
| Meadows | <u>26.30</u> | 21.98 | 81.44 |
| Gravel | <u>0.86</u> | 0.00 | 4.05 |
| Trees | 77.84 | 7.17 | 41.87 |
| Metal sheets | 87.43 | 71.23 | <u>86.77</u> |
| Bare soil | 30.11 | 34.08 | <u>32.63</u> |
| Bitumen | 92.03 | 0.00 | 0.00 |
| Bricks | 79.63 | 93.97 | 84.03 |
| Shadows | 89.14 | 98.57 | 92.12 |
| AA | 60.51 | 46.53 | <u>57.01</u> |
| OA | <u>49.19</u> | 43.86 | 65.35 |
| Kappa | <u>0.42</u> | 0.36 | 0.57 |

Table 2. Quantitative Results of different design approaches of Δ for the Pavia University Image

5. CONCLUSIONS

This work presented an approach to perform clustering directly on the compressed measurements. In particular, we proposed an unsupervised and hierarchical method that takes advantage of Hadamard matrices structure and designs the sensing matrix of the SPC architecture such that the image reconstruction is avoided, enabling to extract clustering features. In general, the presented results showed that overall accuracy of 78.94%, and 65.35% was obtained using the “Salinas”, “Pavia University”, and “Pavia Center” spectral image datasets, respectively.

6. REFERENCES

- [1] Karen Sanchez, Carlos Hinojosa, and Henry Arguello, “Supervised spatio-spectral classification of fused images using superpixels,” *Applied optics*, vol. 58, no. 7, pp. B9–B18, 2019.
- [2] Jorge L Bacca, Carlos A Hinojosa Montero, and Henry Arguello, “Kernel sparse subspace clustering with total variation denoising for hyperspectral remote sensing images,” in *Mathematics in Imaging*. Optical Society of America, 2017, pp. MTu4C–5.
- [3] Mathieu Fauvel, Yuliya Tarabalka, Jon Atli Benediktsson, Jocelyn Chanussot, and James C Tilton, “Advances in spectral-spatial classification of hyperspectral images,” *Proceedings of the IEEE*, vol. 101, no. 3, pp. 652–675, 2012.
- [4] Gonzalo R Arce, David J Brady, Lawrence Carin, Henry Arguello, and David S Kittle, “Compressive coded aperture spectral imaging: An introduction,” *IEEE Signal Processing Magazine*, vol. 31, no. 1, pp. 105–115, 2013.
- [5] Claudia V. Correa, Carlos Hinojosa, Gonzalo R. Arce, and Henry Arguello, “Multiple snapshot colored compressive spectral imager,” *Optical Engineering*, vol. 56, no. 4, pp. 041309, 2016.
- [6] Amir Beck and Marc Teboulle, “A fast iterative shrinkage-thresholding algorithm for linear inverse problems,” *SIAM journal on imaging sciences*, vol. 2, no. 1, pp. 183–202, 2009.
- [7] Mário AT Figueiredo, Robert D Nowak, and Stephen J Wright, “Gradient projection for sparse reconstruction: Application to compressed sensing and other inverse problems,” *IEEE Journal of selected topics in signal processing*, vol. 1, no. 4, pp. 586–597, 2007.
- [8] Joel A Tropp and Anna C Gilbert, “Signal recovery from random measurements via orthogonal matching pursuit,” *IEEE Transactions on information theory*, vol. 53, no. 12, pp. 4655–4666, 2007.
- [9] Carlos Hinojosa, Henry Arguello, and Hoover Rueda, “Analysis of matrix completion algorithms for spectral image estimation from compressive coded projections,” in *2015 20th Symposium on Signal Processing, Images and Computer Vision (STSIVA)*. IEEE, 2015, pp. 1–7.
- [10] Jorge Bacca, Claudia V Correa, and Henry Arguello, “Non-iterative hyperspectral image reconstruction from compressive fused measurements,” *IEEE Journal of Selected Topics in Applied Earth Observations and Remote Sensing*, 2019.
- [11] Nelson Diaz, Carlos Hinojosa, and Henry Arguello, “Adaptive grayscale compressive spectral imaging using optimal blue noise coding patterns,” *Optics & Laser Technology*, vol. 117, pp. 147–157, 2019.
- [12] Yonghao Xu, Bo Du, Fan Zhang, and Liangpei Zhang, “Hyperspectral image classification via a random patches network,” *ISPRS journal of photogrammetry and remote sensing*, vol. 142, pp. 344–357, 2018.
- [13] Carlos Hinojosa, Jorge Bacca, and Henry Arguello, “Coded aperture design for compressive spectral subspace clustering,” *IEEE Journal of Selected Topics in Signal Processing*, vol. 12, no. 6, pp. 1589–1600, 2018.
- [14] Edwin Vargas, Samuel Pinilla, and Henry Arguello, “A fast endmember estimation algorithm from compressive measurements,” in *2018 26th European Signal Processing Conference (EUSIPCO)*. IEEE, 2018, pp. 2210–2214.
- [15] Xun Cao, Tao Yue, Xing Lin, Stephen Lin, Xin Yuan, Qionghai Dai, Lawrence Carin, and David J Brady, “Computational snapshot multispectral cameras: toward dynamic capture of the spectral world,” *IEEE Signal Processing Magazine*, vol. 33, no. 5, pp. 95–108, 2016.
- [16] Marco F Duarte, Mark A Davenport, Dharmpal Takhar, Jason N Laska, Ting Sun, Kevin F Kelly, and Richard G Baraniuk, “Single-pixel imaging via compressive sampling,” *IEEE signal processing magazine*, vol. 25, no. 2, pp. 83–91, 2008.
- [17] H. Garcia, C. V. Correa, and H. Arguello, “Multi-resolution compressive spectral imaging reconstruction from single pixel measurements,” *IEEE Transactions on Image Processing*, vol. 27, no. 12, pp. 6174–6184, Dec 2018.
- [18] Aswin C Sankaranarayanan, Lina Xu, Christoph Studer, Yun Li, Kevin F Kelly, and Richard G Baraniuk, “Video compressive sensing for spatial multiplexing cameras using motion-flow models,” *SIAM Journal on Imaging Sciences*, vol. 8, no. 3, pp. 1489–1518, 2015.
- [19] Ulrike Von Luxburg, “A tutorial on spectral clustering,” *Statistics and computing*, vol. 17, no. 4, pp. 395–416, 2007.
- [20] Humboldt State University Geospatial [Online], “Introduction to remote sensing: Accuracy metrics,” <https://goo.gl/vK2KKj>.